Composition and morphology effects on catalase mimetic activity of potential bioactive glasses

Gianluca Malavasi*, Gigliola Lusvardi

Department of Chemical and Geological Sciences, University of Modena and Reggio Emilia, via Campi 103, 41125, Modena, Italy

A B S T R A C T

The catalase mimetic activity (CMA) of potential bioactive glasses based on Hench - 45S5 Bioglass® ($46.1\%SiO_2$-$24.4\%Na_2O$-$26.9\%CaO$-$2.6\%P_2O_5$ mol%, called H), Kokubo bioactive glass ($50\%SiO_2$–$25\%Na_2O$–$25\%CaO$ mol%, called K) and mesoporous bioactive glass ($80\%SiO_2$–$15\%CaO$–$5\%P_2O_5$ mol%, called MBG) modified by the introduction of metal oxide (MO, M = Ti, V, Mn, Fe, Co, Cu, Zr and Ce) was tested in order to verify how their composition, morphology and synthesis procedure influence the ability to inhibit oxidative stress in terms of decomposition of hydrogen peroxide (H_2O_2), a common reactive oxygen species (ROS).

The characterization was achieved on the glasses before and after the soaking in H_2O_2 in order to obtain information about the kinetic order, the rate and the type of mechanism related to the decomposition H_2O_2 process. In fact, the H_2O_2 decomposition can follow a radical mechanism (with the formation of OH· radical) or a peroxide-complex mechanism. Tests in SBF solutions were performed in order to verify the bioactivity in term of hydroxyapatite (HA) formation.

The introduction of metal oxide into the glass composition promotes the CMA and the better catalytic activities were gained for the Co-, Mn-, Cu-, Ce- and Fe-containing glasses. All these glasses follow a 1st order kinetics but only in the case of Ce-containing glasses (H_4.0Ce) we observe a peroxide-complex mechanism. The Ce-containing glasses preserve their catalytic activity also coated with alginate and the reduction of glass powder dimension enhances the rate of H_2O_2 decomposition. Mesoporous glasses with a high specific surface area show a higher H_2O_2 decomposition rate with respect to that of melt-quenched derived glasses. The introduction of Ce, Cu, V, Ti, Zr and Fe do not modify the bioactivity in terms of HA formation during SBF tests (respect to H bioactive glass) and the alginate coating delay the HA formation without inhibiting its formation. H_5.3Co and H_5.3Mn showed the best catalytic performance (highest *k* value) but they seem not bioactive until 28 days of SBF soaking.

By the data analysis obtained in this manuscript, we can affirm that the Ce-containing glasses are the most promising potential bioactive glasses with antioxidant properties.

1. Introduction

The surgical implantation of biomedical, prosthesis or biomaterial devices in the body, usually causes an unhealthy process of inflammation [1,2]. During inflammation (i.e. the complex biological response of body tissues to harmful stimuli), an excessive increase in the production rate of Reactive Oxygen Species (ROS) occurs, which can cause oxidative stress that is responsible for damaging nucleic acids, proteins, and lipids in cell membranes and plasma lipoproteins [3]. This oxidative stress mechanism is defined as the unbalance between the proliferation of highly reactive free radicals in the body and the antioxidant activity of some enzymes (e.g., superoxide dismutase (SOD), catalase (CAT),

and glutathione peroxidase (GSH-Px)) that converts them into non-dangerous species [4–6]. Because of this unbalance, the times of complete post-surgery recovery could be lengthened [7,8]. Also, the use of drugs with antioxidant characteristics, such as propofol, local anaesthetics, calcium channel blockers, and steroids, has been reported to have potential to reduce oxidative stress and their administration may improve the postoperative clinical course [9].

Between biomaterial devices, bioactive glasses play a fundamental role in the hard tissue engineering [10]. The first bioactive glass, later termed 45S5 Bioglass®, was synthesized by Larry Hench in 1969. Its first clinical application was in 1985, when it was used for the treatment of conductive hearing loss by replacing the bones of the middle

---

ear [11,12]. Hench discovered that this phospho-silicate glass forms a bond with bone strong enough to not be able to be removed without breaking the bone itself; moreover, it stimulates new bone growth away from the bone-implant interface [13].

The bone bonding ability (bioactivity) is due to a complex bio-chemical process. The first process that takes place is the dissolution of the glass structure at the interface with body fluids and the subsequent formation of a calcium phosphate (hydroxyapatite, $Ca_5(PO_4)_3OH$, HA) layer on the glass surface, which occurs in the first few hours after implantation. This HA is usually carbonate-substituted (hydroxycarbonate apatite, HCA) [10] and is chemically similar to the inorganic phase of the human bone.. [14]. Subsequently, the interaction of collagen fibrils from host bone via cellular processes (osteoblasts) with the HCA layer, creates a strong bone bonding. The mechanism of glass dissolution plays a key role in the expression of bioactivity, allowing space for tissue regrowth and actively stimulating cells to produce new tissue. The dissolution rate of a glass in biological fluids firstly depends on its surface structure, that is directly related to its chemical composition. Hench identified the compositional limits for bone and soft tissue bonding in the SiO_2–Na_2O–CaO–P_2O_5 glass system, showing the best composition as 46.1%SiO_2-24.4%Na_2O-26.9%CaO-2.6P_2O_5 mol% [15].

One trend in the development of bioactive glasses is the incorporation of several ions able to enhance physical and therapeutic properties of the bioactive glasses [16], such as antibacterial activity (Ag [17,18], Ga [19,20]), stimulation of bone development and maintenance (Mg [21], Mn [22,23], Cu [24], Sr [25], Zn [26,27], Co [28]), fluorapatite precipitation (F [29,30]), mechanical properties (K [31]), reduction of local oxidative stress (Ce [32], Sr [33]) and magnetic local heater for tumours treatment (Fe [34]).

In particular in the last 5-years, it was demonstrated that the presence of Ce^{3+}/Ce^{4+} ions on the bioactive glass surface is able to promote the enzymatic-like (SOD and CAT) activity reducing the oxidative stress [35,36]. This ability is strictly correlated to the ability of the redox Ce^{3+}/Ce^{4+} interconversion, such as detected in the case of CeO_2 nanoparticles (CeONPs or nanoceria). In fact, nanoceria have received much attention because of their excellent catalytic activities, which are derived from quick interconversion between Ce^{4+} and Ce^{3+} oxidation states. The surface of the nanoparticles exhibit oxygen vacancies in the lattice structure; these arise through loss of oxygen atoms, alternating between CeO_2 and CeO_{2-x} during redox reactions [37,38].

The CAT mimetic activity, otherwise the ability to catalyze the decomposition reaction of H_2O_2, was demonstrated also for other metallic nano-oxides [39]. For example, Gu et al. showed that iron oxide nanoparticles (both Fe_3O_4 and Fe_2O_3) exhibited dual enzyme mimetic properties including CAT and peroxidase [40]. Also in this case is the presence of iron ions able to promote the H_2O_2 decomposition, in fact studies conducted at low pH has predominantly stemmed from the discovery by Fenton [41] that a mixture of a ferrous salt and hydrogen peroxide possessed potent oxidising properties not present in the separate reagents [42].

Subsequent studies have interpreted the catalytic H_2O_2 decomposition of iron in terms of a free radical or a complex mechanism. The radical mechanism, first proposed by Haber and Weiss [43] and later modified by a number of workers [44], involves the formation of radical species such as $HO_2\cdot$ and $HO\cdot$. The complex mechanism proposed by Kremer [44] assumes that complexes and compounds of iron and peroxide are intermediates in the reaction. While numerous attempts have been made to distinguish between these two concepts, there is still some doubt as to which mechanism actually operates and several factors influence the mechanism, in particular the pH [45].

In view of this, in the present work we synthetized potential bioactive glasses based on the composition of 45S5 Bioglass® (46.1% SiO_2-24.4%Na_2O-26.9%CaO-2.6P_2O_5 mol%, called H) and 50% SiO_2–25%Na_2O–25%CaO mol% (called K) modified by metallic oxides (oxides of Ti, V, Mn, Fe, Co, Cu, Zr and Ce) with potential enzymatic-

Table 1
Nominal composition (mol%) of the studied glasses.

Glasses	SiO_2 (% mol)	Na_2O (% mol)	CaO (% mol)	P_2O_5 (% mol)	MO (% mol)
H	46.1	24.4	26.9	2.6	–
H_5.3Ti	43.6	23.1	25.5	2.5	5.3
H_5.3V	43.6	23.1	25.5	2.5	5.3
H_5.3Mn	43.6	23.1	25.5	2.5	5.3
H_5.3Fe	43.6	23.1	25.5	2.5	5.3
H_5.3Co	43.6	23.1	25.5	2.5	5.3
H_5.3Cu	43.6	23.1	25.5	2.5	5.3
H_5.3Zr	43.6	23.1	25.5	2.5	5.3
H_5.3Ce	43.6	23.1	25.5	2.5	5.3
H_4.0Mn	44.3	23.4	25.8	2.5	4
H_4.0Fe	44.3	23.4	25.8	2.5	4
H_4.0Co	44.3	23.4	25.8	2.5	4
H_4.0Cu	44.3	23.4	25.8	2.5	4
H_4.0Ce	44.3	23.4	25.8	2.5	4
K	50.0	25.0	25.0	–	–
K_3.6Ce	48.2	24.1	24.1	–	3.6
MBG	80.0	–	15.0	5.0	–
MBG_5.3Ce	75.8	–	14.2	4.7	5.3

like activity in order to detect the effect of glass composition on the potential CAT mimetic activity. In addition, the influence of glass synthesis techniques (melt-quenching and sol-gel) and morphology (fine and coarse powders and alginate-coated powders) on potential CAT mimetic activity was evaluated. The kinetic of H_2O_2 decomposition was also investigated.

2. Materials and methods

2.1. Synthesis by melt-quenching method

Two series of bioactive glasses, called H and K series, added with variable percentages of metallic oxides have been synthesized *via* the melting method [46]. The nominal composition of prepared glasses are reported in Table 1. The metallic oxide amount was expressed as MO (M = Ti, V, Mn, Fe, Co, Cu, Zr and Ce) independently of the raw material used in the synthesis; in this way it is possible to evaluate and compare the effect of metal on the glass properties.

As a function of composition, the samples were prepared by mixing reagent grade SiO_2, Na_2CO_3, $CaCO_3$, $Na_3PO_4 \cdot 12H_2O$ (this last compound only for H glass series), and TiO_2, NH_4VO_3, $MnCO_3$, Fe_2O_3, $(CH_3COO)_2Co$, CuO, ZrO_2 and CeO_2 in an agate mortar. The maximum amount of CeO_2 that enables to obtain an amorphous sample is 5.3 mol % for H series and 3.6 mol% for K-based [47]. For comparison purpose, we decided to add to the H-based composition 5.3 mol% of each MO.

Then each batch was put into a Pt crucible, and melted in an electric oven. The heating ramp was set to 15 °C/min up to 1000 °C and 8 °C/min up to 1350 °C. Samples were maintained at this temperature for 2 h, to ensure optimal melting and mixing of all the oxides, and finally quenched at room temperature on a graphite plate. The obtained glasses were homogeneous and transparent. Finally, the glasses were gently milled in an agate mortar and sieved in order to obtain powders in the range of 250–500 μm (coarse powders), 125–250 μm (medium powders) and lower than 250 μm (fine powders).

2.2. Synthesis of Ce-containing mesoporous bioactive glasses by sol-gel & EISA method

The synthesis was obtained via sol gel method with the application of the evaporation induced self-assembly process (EISA) using the non-ionic surfactant Pluronic P123 as a structure-directing agent (SDA). This procedure permits to obtain a material characterized by the presence of mesoporous, in fact we called these systems mesoporous bioactive glasses (MBG). The details of the synthesis and glass

characterization were reported in ref. 32. In brief, tetraethyl orthosilicate (TEOS), triethyl phosphate (TEP), calcium nitrate tetrahydrate $Ca(NO_3)_2 \cdot 4H_2O$ and cerium nitrate hexahydrate $Ce(NO_3)_3 \cdot 6H_2O$ were used as SiO_2, P_2O_5, CaO and CeO_2 oxides sources, respectively. Firstly the surfactant Pluronic P123 (4.5 g) was dissolved by magnetic stirring in 85 mL of ethanol containing 1.2 mL of 10% HCl solution; afterward the appropriate amounts of TEOS, TEP, $Ca(NO_3)_2 \cdot 4H_2O$ and $Ce(NO_3)_3 \cdot 6H_2O$ were added, under continuous stirring in 3 h intervals at room temperature. The resulting sols were kept under stirring overnight and then cast in Petri dishes to undergo EISA process. After 4 days, the dried gels were removed as homogeneous and transparent membranes and heated at 700 °C for 3 h under an air atmosphere to remove the surfactant and nitrate groups, as well as to stabilize the resultant mesoporous glasses. Finally, the MBGs were gently milled and sieved at a mean dimension lower than 250 μm. The nominal molar compositions of the samples are reported in Table 1 and named hereafter MBG with the relative mol% of CeO_2.

2.3. Preparation of alginate-coating

In order to develop a biocompatible scaffold that supports the particles of potential bioactive glass to promote a fast degradation of H_2O_2 reducing the oxidative stress, we have prepared Ca-alginate coating of bioactive glasses (beads).

An aqueous solution with a Ca^{2+} concentration of 0.1 mol/L was prepared by dissolving calcium chloride ($CaCl_2 \cdot 2H_2O$) in a backer. A second aqueous solution, (~1% wt) of sodium alginate, (empirical formula $NaC_6H_7O_6$) was added under stirring to the powdered glass (lower than 250 μm (fine powders), with weight ratio, sodium alginate/glass, of 0.4; an opaque suspension was obtained that was maintained under continuous stirring to avoid a phase separation. Withdrawals (30mL) of the suspension were dropped into 250 mL of the calcium chloride solution under slow stirring. Spherical beads deposited on the bottom of the backer, they were filtered off under vacuum and washed with denaturised ethanol, their mean diameter was ≈4 mm, after washing the beads were dried at 60 °C, (2h), after drying the beads diameter was ≈2 mm. The beads were formed with the glassy powders coated by calcium-alginate; for this reason, the samples prepared were denoted by "B_" before the name of the glass sample used [32].

Glass-free calcium alginate beads, (abbreviated as B_algCa) were also prepared as a reference, by dropping the solution of sodium alginate (30mL) into the calcium chloride solution. The beads were named as: B_H_5.3Ce, B_K_3.6Ce and B_MBG_5.3Ce.

In order to quantify the alginate/glass weight ratio of the beads, mass-loss analysis was performed on each bead samples. A precise number of beads was weighted into a small platinum crucible, put into an oven up to 1000 °C with a heating rate of 10 °C/min; an isotherm of 5 min and cooling intervals 5 min long were performed, after every cooling intervals the sample was weighted. The analysis was performed in triplicate. On the basis of the results, the glass to be weighted for catalase activity and bioactivity tests was determined.

2.4. Catalase mimetic activity (CMA) tests

In order to verify the effect of the glass composition, the glass particles dimension, the synthesis procedures and the alginate coating toward the catalase mimetic activity (hereafter abbreviated as CMA), the samples were soaked, under continuous stirring at 37 °C in a solution of 1.00 mol/L H_2O_2 previously standardized with $KMnO_4$. The soaking time was set to 1, 2, 4, 8, 24, 48, 96 and 168 h. In all samples, a constant mass(glass)/volume(solution) ratio of 5mg/mL was maintained. In the case of alginate coated samples, we soaked a quantity of beads containing about 100 mg of glasses and 20mL of 1 mol/L H_2O_2.

For comparison purposes, a sample containing 70 mg of B_algCa and 20mL of 1.00 mol/L H_2O_2, was prepared. After soaking, the samples were filtered and dried overnight at 60 °C; whereas the solutions were

titrated by $KMnO_4$ to determine the residual H_2O_2. Before titrations, the pH value of the filtered residual H_2O_2 solutions was measured. The residual H_2O_2 concentration was the mean value of 3 independent replicas and the deviation standard was always ≤0.03 mol/L.

After removing from the H_2O_2 solution at different times and drying, the glassy powders (diameter lower than 250 μm) of H_4.0Mn, H_4.0Fe, H_4.0Co, H_4.0Cu and H_4.0Ce samples were immersed in a freshly prepared 1.00 mol/L H_2O_2 solution for 4 h to verify the ability of the glasses to further degrade H_2O_2 in a second reuse.

2.5. CMA test with t-BuOH as radical scavenger

t-BuOH is an often applied OH· scavenger in scientific investigations [48], because it reacts with OH· with a substantially high rate constant forming a non-reactive radical (t-BuOH·). This additive has negligible reactivity with H_2O_2, so we added 15 mL of t-BuOH during the CMA test in order to verify the decrease of H_2O_2 concentration if the decomposition occurs by a radical mechanism with OH· radical production [43,44].

2.6. Determination of kinetic parameter k

The decomposition H_2O_2 reaction can be studied from the kinetic point of view, if we consider an isothermal reactor and a constant concentration of catalyzer, the kinetic equation that describes the decomposition is:

$$- \frac{d[H_2O_2]}{dt} = k[H_2O_2]^n$$

where k is the rate constant and n the reaction order. We tried to fit our data using $n = 0$ (order 0), $n = 1$ (1st order) and $n = 2$ (2nd order). On the basis of linear regression coefficient (R^2) of the fitting line we determine better n value.

2.7. UV–vis spectroscopy

To perform a qualitative estimation of the redox nature of metal ions contained in the glassy samples, UV–vis analyses were carried out on the as quenched glasses and on the samples reacted in 1 mol/L H_2O_2. Spectra were acquired in the 200–800 nm range, with a UV-VIS-NIR (JASCO V-570) spectrophotometer. The diffuse reflectance technique with a $BaSO_4$ plate as reflectance standard was used.

2.8. Bioactivity tests

The bioactivity tests in Simulated Body Fluid (SBF) were performed as reported in ref. 48. We soaked 150 mg of glassy powders (dimension lower than 250 μm) or 250 mg of beads corresponding to 150 mg of glass, in 100 mL of SBF for 28 days and then, we filtered the solutions, washed the glass powders or beads with acetone- The samples were analysed by means of the FT-IR technique to evaluate the formation of hydroxyapatite (HA) on their surface. Infrared spectra were performed on KBr pellets before and after soaking in SBF. As a reference the spectrum of B_algCa was also collected. The spectra were collected with a FT-IR JASCO-4700 instrument in the range 400–2000 cm^{-1}.

3. Results

Fig. 1 reports the residual H_2O_2 concentrations after different soaking times of the H series glasses modified with 5.3% of MO and with powders diameter lower than 250 μm (fine powders). The concentration of starting solution of H_2O_2 solution is 1.00 mol/L.

In all cases, from the inspection of Fig. 1, it can be asserted that the presence of MO increases the rate of H_2O_2 decomposition, while H shows a negligible ability to degrade H_2O_2. The glass systems containing MO can be divided into two groups: i) the first one, comprising
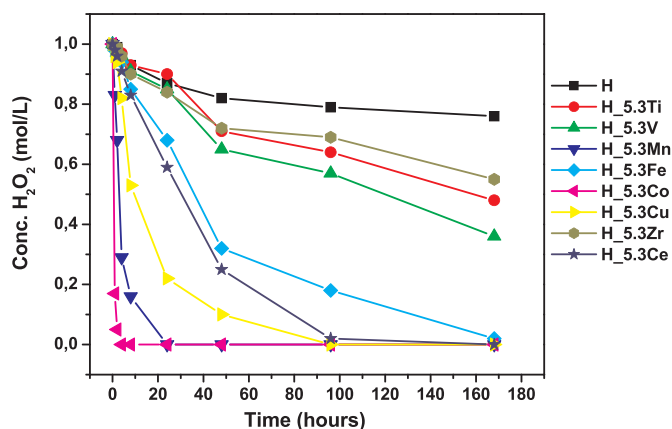
Fig. 1. Molar concentration (mol/L) of H_2O_2 solution before and after immersion of series glasses modified with 5.3% of metal oxides, with powder dimension lower than 250 μm (fine powders), in 1.00 mol/L H_2O_2 solution. (Standard Deviations calculated on three independent replicates are ≤0.03mol/L).

of H_5.3Co, H_5.3Mn, H_5.3Cu, H_5.3Ce and H_5.3Fe, in 168 h degrades completely H_2O_2; ii) the second one consisting of H_5.3V, H_5.3Ti and H_5.3Zr decreases the H_2O_2 concentration of 40–60% in 168 h.

The results obtained by the CMA tests reported in Fig. 1 suggest that Co, Mn, Cu, Ce and Fe ions present in the glass structure catalyze extremely H_2O_2 decomposition. In view of these results, we perform CMA tests with the glasses modified by 4.0 mol% of the above-mentioned MO; these tests were performed with the addition to the H_2O_2 1mol/L solution of t-BuOH in order to render ineffective the OH· radical, developed during the H_2O_2 decomposition, if it occurs through a radical mechanism. The results are reported in Fig. 2 and it is possible to note that the presence of t-BuOH decreases the rate of H_2O_2 concentration decrement for the Mn, Co, Fe and Cu-containing glasses. In the case of H_4.0Ce sample the H_2O_2 decrease is the similar in presence/absence of t-BuOH.

In Fig. 3 are reported the results of the CMA tests, where we have investigated the effect of morphology of the glasses as a function of i) glassy powder dimensions (Fig. 3, section a) and ii) the porosity (Fig. 3, section b). The size distribution of samples was checked by laser
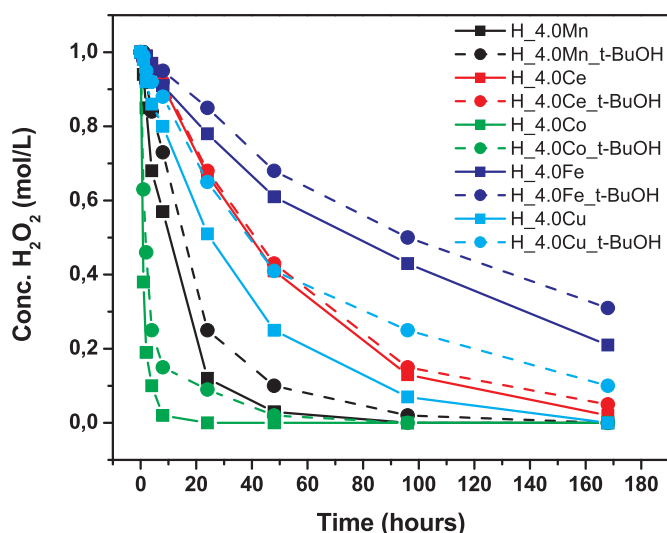

Fig. 2. Molar concentration (mol/L) of H_2O_2 solution before and after immersion of H_4.0Mn, H_4.0Ce, H_4.0Co, H_4.0Fe and H_4.0Cu with powder dimeter lower than 250 μm (fine powders), in 1.00 mol/L H_2O_2 solution (■) and 1.00 mol/L H_2O_2 solution + t-BuOH (●). (Standard Deviations calculated on three independent replicates are ≤0.03mol/L).

diffraction grain size measurements (data reported in Fig. S1, Supplementary Materials). The results confirm that it is possible to classify the size range as fine, medium and course.

Decreasing the glass dimensions (Fig. 3, section a), we observe an increment of the H_2O_2 decomposition rate, suggesting that the catalytic process takes place at the interface between the glass surface and the H_2O_2 solution. Similar effects can be derived from the data reported in Fig. 3 section b; in fact, the glass obtained by melt-quenching techniques present a very low porosity while the mesoporous glasses present a high amount of mesoporous with a consequent high specific surface area.

The presence of alginate coating (Fig. 3, section c) causes a reduction in the H_2O_2 degradation rate for the melt-quenched glasses (H_5.3Ce and K_3.6Ce), while seem do not influence the catalytic performance of mesoporous glass (MBG_5.3Ce). The alginate (beads) is not able to promote the H_2O_2 degradation over 168 h of contact.

The H_2O_2 degradation trends were fitted using the kinetic equations of zero ($[H_2O_2]_0 - [H_2O_2]_t$ vs t), 1st ($-\ln\left(\frac{[H_2O_2]_t}{[H_2O_2]_0}\right)$ vs t) and 2nd ($\left(\frac{1}{[H_2O_2]_t} - \frac{1}{[H_2O_2]_0}\right)$ vs t) order. The best fitting result (linear regression coefficient R) defines the more probable reaction order. The fitting equation parameter and R are reported in Table S1 (Supplementary Materials) for H glass series modified by metal oxides. The slope of the linear fitting represents k, the decomposition rate constant. The better R values of H, H_5.3Ti and H_5.3Zr are relatives of 2nd order kinetics, while for the others samples a 1st order kinetic seem more feasible. In fact, the dependence of H_2O_2 decomposition vs time for H_5.3Co/Mn/Cu/Fe/V glasses is satisfactorily described by an exponential trend, suggesting a 1st order reaction.

Fig. 4 reports the k values: the higher k values were determined for 1st order kinetic, while the 2nd order kinetics gives rise to a lower k value. Interesting to note that the best performance, in term of decomposition rate, was obtained by the H glass modified by cobalt oxide.

In Table 2 are reported the H_2O_2 concentrations after 4 h of glass soaking after a 2nd immersion); in general, the concentrations of H_2O_2 after 2nd immersion are lower with respect to those after 1st immersion (Δ > 0, see Table 2). This means that all glasses preserve the ability to catalyze the H_2O_2 decomposition in a second reuse. However, for the H_4.0Fe and H_4.0Ce, this last in particular, the H_2O_2 concentration decrement is more pronounced suggesting that the catalytic performances of these two glasses substantially increases in the 2nd immersion.

In Fig. 5 are reported the UV–Vis spectra in the range 200–800 nm of H glass series modified by 5.3 mol % of metal oxide.

The spectra of H glass (Fig. 5 (a)) do not show significative bands in the Vis region and there is not substantially modifications before and after the CMA tests in H_2O_2; it is only present a band in the 270 nm region attribute to soda-lime silicate glasses [49]. In the case of H_5.3Ti (Fig. 5 (b)) and H_5.3Zr (Fig. 5 (h)) samples no significative differences were observed with respect to H glass.

In the case of H_5.3V glass (Fig. 5 (c)) a band in the range 250–350nm appear and this can be attributed to the 340 nm characteristic band of V^{5+} in the glass [49] which remains unchanged even after 168 h of H_2O_2 contact. The presence of V^{3+} ions in the glass structure can be excluded since there is no characteristic 645 nm absorption while the presence of V^{4+}, which absorbs at 1100 nm, is not excluded [49].

The Mn containing glass (Fig. 5 (d)) is characterized by the band attributed to Mn^{3+} (around 500 nm), while the absorption band of Mn^{2+} (400–430 nm) is not clearly visible. This is probably due to very low molar absorption coefficient of Mn^{2+} band that is due to the spin forbidden $^6A_1 \rightarrow {}^4A_1$, whereas Mn^{3+} band presents molar absorption coefficient about 100 times more intense than Mn^{2+}. During the H_2O_2 soaking the spectra show an increment of absorbance in the 400–430 nm zone probably due to partial reduction on Mn^{3+} to Mn^{2+}.
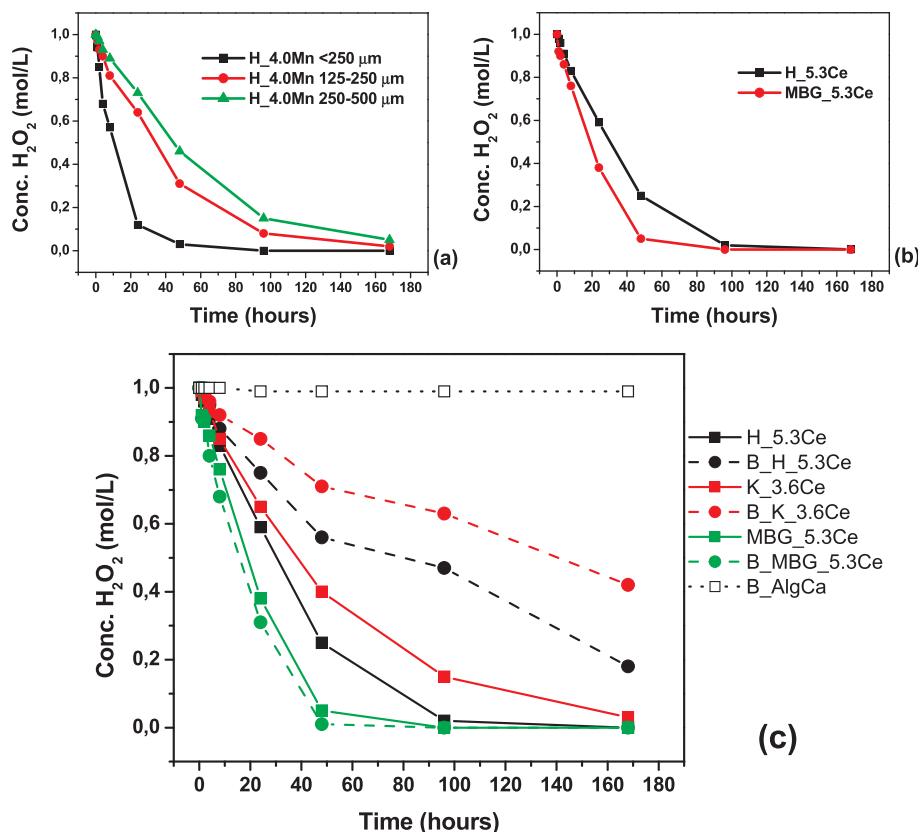
Fig. 3. Molar concentration (mol/L) of H_2O_2 solution before and after immersion in 1.00 mol/L H_2O_2 solution of: (a) H_4.0Mn with powder dimension lower than 250 μm (fine powders), in the range125–250 μm (medium powders) and in range 250–500 μm (coarse powders); (b) H_4.0Mn synthesized by melt-quenching technique and MBG_5.3Ce synthetized by EISA sol-gel methods; (c) H_5.3Ce, K_3.6Ce and MBG_5.3Ce glass powders with (●) and without (■) alginate coating. (Standard Deviations calculated on three independent replicates are ≤0.03mol/L).
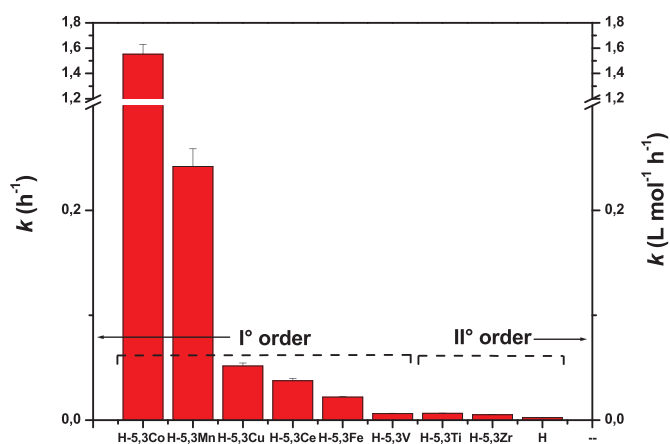

Fig. 4. k values calculated for the H_2O_2 decomposition process.

The spectra of H_5.3Fe samples before and after H_2O_2 immersion (Fig. 5 (e)) show the bands attributed to Fe^{3+} ions in the glass network in the range 380–450 nm in the sodium-silicate glasses, however, it is not possible to confirm the presence of Fe^{2+} since it has no absorption in the UV–Vis range, in fact Fe^{2+} ions adsorb in the NIR region at 1050 nm.

For Co-containing glasses (H_5.3Co, Fig. 5 (f)) it can be noted the bands at 530, 590 and 645 nm characteristic of Co^{2+} in tetrahedral geometry. These bans are still present after 168 h of H_2O_2 soaking, but in the region < 450 nm decrease the band cantered at 360 nm attributed to Co^{3+} in tetrahedral geometry [50]. From this result, we can suggest a partial reduction of Co^{3+} to Co^{2+} during the H_2O_2 decomposition.

In Fig. 5 (g) it is possible to see a wide band at 780 nm, it is characteristic of the glasses containing Cu^{2+} ions in distorted octahedral geometry. This band do not significantly change during the CMA test. It is not possible exclude the presence Cu^+ ions in the glass network since its electronic configuration d [10] does not provide transitions in the UV–visible range [49].

In a previous work [35], we have verified that Ce^{3+} absorbs in the range 250–300 nm, while Ce^{4+} absorbs in the range 350–400 nm. Thus, with the spectra reported in Fig. 5 (i) it is possible to gain qualitative information about the oxidation state of cerium during the H_2O_2 reaction. It is possible to notice that after soaking (H_5.3Ce_168h), the samples show an increase in the value absorbance in the range 350–450 nm suggesting an increment of Ce^{4+} content in the glass.

In Fig. S2 there are the spectra of H_4.0 M (M = Mn, Fe, Co, Cu and Ce) glasses after the H_2O_2 soaking for 168 h with or without the addition of t-BuOH as radical scavenger. The spectra of each glass are very similar, suggesting that the OH· radical scavenger does not substantially modify the redox behaviour of metal ions in the glass structure.
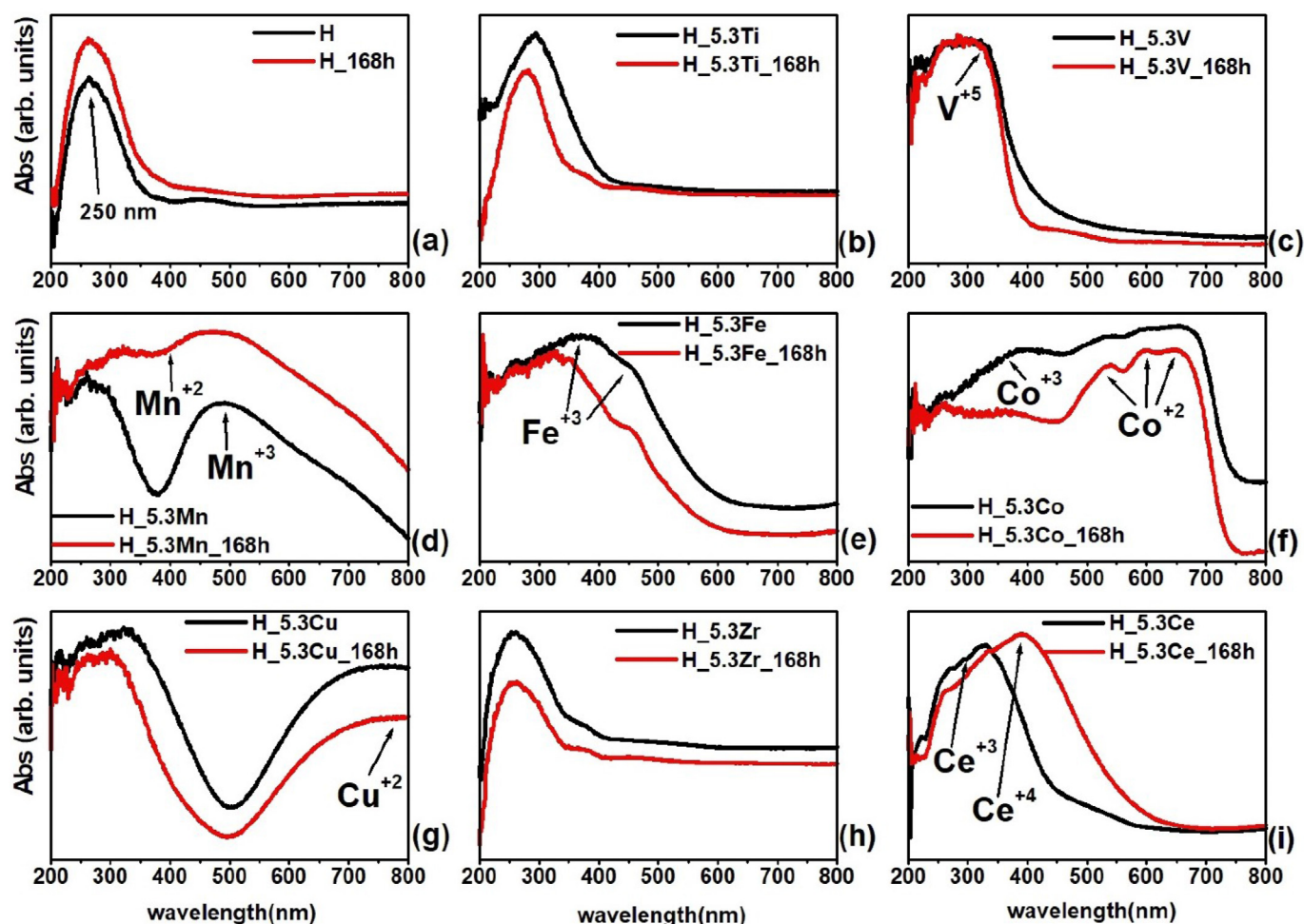
Fig. 6 reports the FT-IR absorption spectra of H and H-based glasses modified by metal oxides (M = Ti, V, Mn, Fe, Co, Cu, Zr and Ce) before and after 28 days of SBF soaking (bioactivity tests).

During the bioactivity tests, several processes take place and FT-IR analysis can be utilized in order to analyse the overall process. The glass cation leaching (Na^+ and Ca^{2+}) and the formation of an amorphous silica gel layer (increment of material surface area) on the glass surface are related to the appearance of two bands at 1140-1270 cm^{-1} and 800 cm^{-1}, associated to Si–O–Si stretching and Si–O–Si bending respectively, and the simultaneous increase of bridging oxygens (BO) band absorption and decrease of non-bridging oxygens (NBO) bands absorption (900 and 870 cm^{-1}) with soaking [51]. This process take place for H, H_5.3V, H_5.3Fe, H_5.3Cu and H_5.3Ce. The formation of a crystalline HA apatite layer is an index of *in vitro* bioactivity and it related to the appearance of two peaks at 560-565 cm^{-1} and 600-605 cm^{-1} and a sharp band at 1035-1050 cm^{-1} not easy to distinguish it

Table 2

Molar concentration (mol/L) of H_2O_2 solution after 2nd immersion (4 h) in a freshly 1 mol/L H_2O_2 solution ($\Delta = [H_2O_2]_{t=x}1^{st}_{immersion} - [H_2O_2]_{t=4h} 2^{nd}_{immersion}$).

Glass (-t = x)	$[H_2O_2]_{t=4h} 2^{nd}_{immersion}$ (mol/L)	Δ (mol/L)	Glass (-t = x)	$[H_2O_2]_{t=4h} 2^{nd}_{immersion}$ (mol/L)	Δ (mol/L)
H_4.0Fe-1h	0,96	+0,01	H_4.0Mn-1h	0,67	+0,01
H_4.0Fe-2h	0,95	+0,02	H_4.0Mn-2h	0,68	0,00
H_4.0Fe-4h	0,94	+0,03	H_4.0Mn-4h	0,70	−0,02
H_4.0Fe-8h	0,88	+0,09	H_4.0Mn-8h	0,69	−0,01
H_4.0Fe-24h	0,87	+0,10	H_4.0Mn-24h	0,69	−0,01
H_4.0Fe-96h	0,86	+0,11	H_4.0Mn-96h	0,70	−0,02
H_4.0Fe-168h	0,84	+0,13	H_4.0Mn-168h	0,62	+0,06
H_4.0Co-1h	0,09	+0,01	H_4.0Cu-1h	0,86	0,00
H_4.0Co-2h	0,09	+0,01	H_4.0Cu-2h	0,86	0,00
H_4.0Co-4h	0,11	−0,01	H_4.0Cu-4h	0,84	+0,02
H_4.0Co-8h	0,09	+0,01	H_4.0Cu-8h	0,84	+0,02
H_4.0Co-24h	0,09	+0,01	H_4.0Cu-24h	0,83	+0,03
H_4.0Co-96h	0,08	+0,02	H_4.0Cu-96h	0,84	+0,02
H_4.0Co-168h	0,08	+0,02	H_4.0Cu-168h	0,81	+0,05
H_4.0Ce-1h	0,97	0,00			
H_4.0Ce-2h	0,97	0,00			
H_4.0Ce-4h	0,95	+0,02			
H_4.0Ce-8h	0,91	+0,06			
H_4.0Ce-24h	0,83	+0,14			
H_4.0Ce-96h	0,74	+0,23			
H_4.0Ce-168h	0,60	+0,37			

Fig. 5. UV–Vis absorption spectra before and after immersion in H_2O_2 (1.00 mol/L) for 168 h of (a) H; (b) H_5.3Ti; (c) H_5.3V; (d) H_5.3Mn; (e) H_5.3Fe; (f) H_5.3Co; (g) H_5.3Cu; (h) H_5.3Zr and (i) H_5.3Ce glasses.

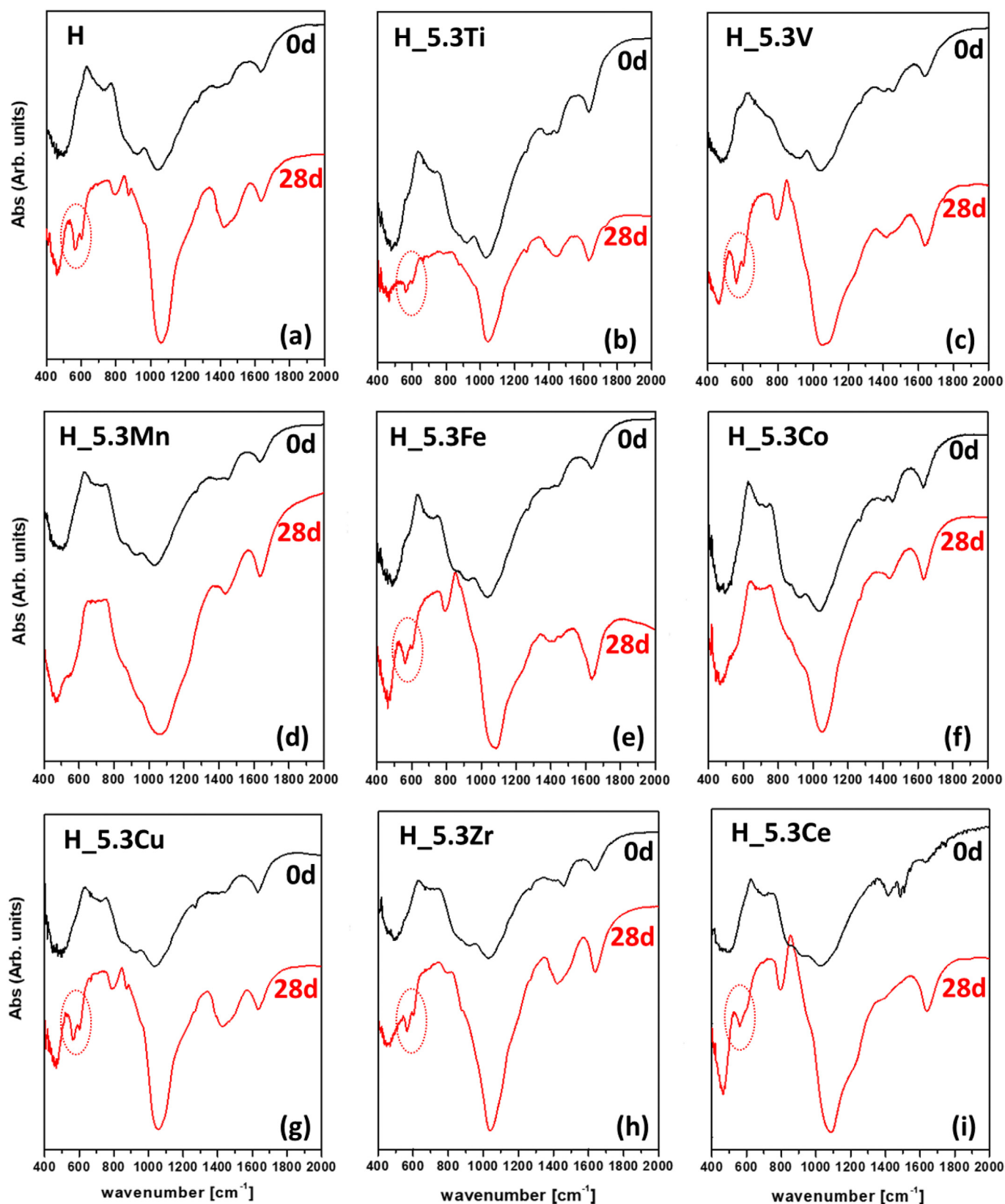**Fig. 6.** FT-IR absorption spectra of (a) H; (b) H_5.3Ti; (c) H_5.3V; (d) H_5.3Mn; (e) H_5.3Fe; (f) H_5.3Co; (g) H_5.3Cu; (h) H_5.3Zr and (i) H_5.3Ce glasses before and after 28 days of SBF soaking.
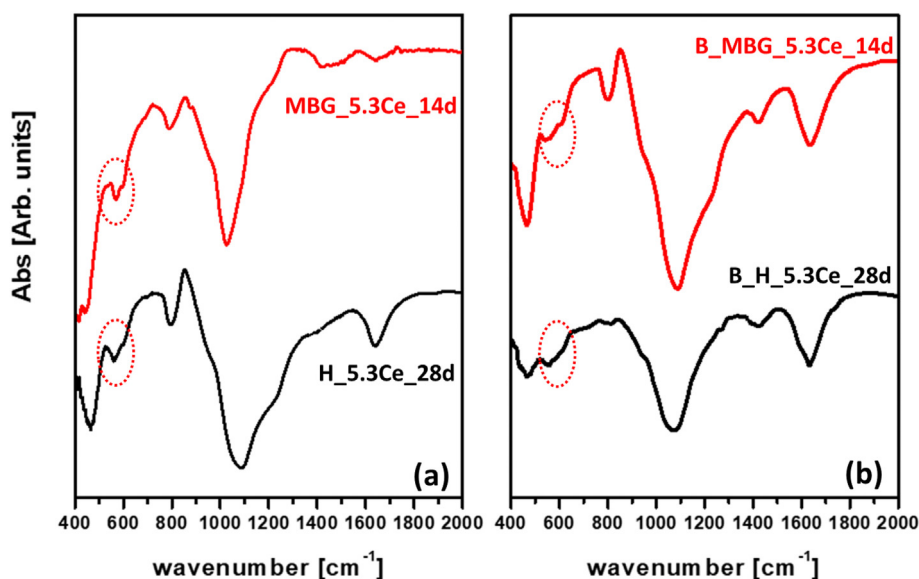
Fig. 7. FT-IR absorption spectra (a) H _5.3Ce after 28 days and MBG_5.3Ce after 14 days of SBF soaking; (b) B_H _5.3Ce after 28 days and B_MBG_5.3Ce after 14 days of SBF soaking.

from the BO band at 1000 cm^{-1} [52]. From Fig. 6 it is possible to see these bands at 560-565 cm^{-1} and 600-605 cm^{-1} after 28 days of soaking for H, H_5.3Ti, H_5.3V, H_5.3Fe, H_5.3Cu, H_5.3Zr and H_5.3Ce glassy samples. While for H_5.3Co and H_5.3Mn glasses there are no evidence of silica gel layer and HA formation.

Modify the synthesis procedure, it is possible to see that the peaks at 560-565 cm^{-1} and 600-605 cm^{-1} attributed to the formation of a crystalline HA apatite layer appear at shorted time (14 days) in the case of MBG_5.3Ce glasses (Fig. 7 section a), while the alginate coating seems do not influence the bioactivity of the sample in term of HA formation, however the two peaks in this last case seem less intense and definite (Fig. 7 section b) with respect to the sample without the alginate coating.

4. Discussion

The present results show that the CMA is strictly related to the glass composition. The H_2O_2 degradation rate is very low in the case the H glass; this glass is formed by only SiO_2, CaO, Na_2O and P_2O_5 and no transition metal oxides are present in the glass composition. The decomposition of hydrogen peroxide vapor on relatively inert surfaces such as silicate glasses was investigated and the results showed the efficacy of sodium-calcium-silicate glasses containing up to 14.2 mol% of Na_2O and 6.3 mol% of CaO and PbO. However, for this glass system the presence of lead that act as active centres for hydrogen peroxide decomposition seem fundamentals [53]. Recent studies revealed that various solid nanometric oxide particles are also effective, such as SiO_2, Al_2O_3, TiO_2, CeO_2 and ZrO_2 [54]. First-order kinetics were observed for the decomposition in all cases. The type of oxide had a strong effect on the decomposition rate term with increasing rate in the order of $SiO_2 < Al_2O_3 < TiO_2 < CeO_2 < ZrO_2$ [54]. The rate coefficient for H_2O_2 decomposition increases with increasing surface area of the oxide, but the number or efficiency of reactive sites rather than the total surface area may have the dominant role. These results agree with our finding, in fact H glass shows a 1st order kinetics and the lowest decomposition rate constant k with respect to the other glasses. Moreover, also H_5.3Ti, H_5.3Zr show a 1st order kinetic as reported in ref. 54. However, the behaviour of Ce-containing glass (H_5.3Ce) in our study seem be better explained by 2nd order kinetic.

In several previous works, the ability of metal catalyst systems to decompose peroxide has been reported to be closely linked to their

individual electrochemical behaviour: the metal must exist in two oxidation states having a suitable redox potential such that the lower oxidation state can be oxidized by peroxide and the higher oxidation state reduced by it [44,55,56]. For these regions, the better performance, in term of the decomposition rate constant k determined for the H_2O_2 decomposition process, obtained in our work (Fig. 4) are of the Co, Mn, Cu, Ce, Fe and V-containing glasses with respect to the glass non-containing metal ions with two oxidation state (H, H_5.3Ti and H_5.3Zr).

While electronic considerations have been found to be important in determining the activity of metal catalysts, a number of other factors are also considered to be important. The activities of metal catalysts have been shown to be strongly dependent on the reaction conditions used such as temperature and pH. For example, the effects of pH in particular have been studied in considerable detail, with different metal ions found to behave differently as a function of pH [57]. In the pH range 7–10, Brown & Abbot [58] proposed that the performance of metal ions (homogeneous catalysis) in the degradation of H_2O_2 solution are $Co^{+3} > Mn^{2+} > Cu^{2+} > Fe^{3+}$. This trend is in perfect agreement with of finding, although the data relating to the Ce and V ions are not present in the ref. 58.

The decomposition of hydrogen peroxide followed 1st order kinetics in the presence of Fe- and Mn-containing sands [56]. In this paper, it is interesting to note that the sands Fe-rich (Mn-poor) present a k value in the range $2.06–1.95 \cdot 10^{-3}$ min^{-1} while the sand Mn-rich present a k value in the range $2.02 \cdot 10^{-2}$ min^{-1} suggesting an higher catalytic activity of Mn ions with respect to Fe ions. The same kinetic order and trend is observed in the present study, in fact, passing from H_5.3Fe glass to H_5.3Mn, the k value increases of one magnitude order (0.02196 h^{-1} vs 0.242 h^{-1}, respectively).

Table 3
Decomposition rate constant k determined for the H_2O_2 decomposition process (1st order kinetic) in presence/absence of t-BuOH.

Glass	K (h^{-1})	$k_{inhibition}$ ($+t$-BuOH) (h^{-1})	$\Delta\%_{inhibition}$
H_4.0Co	0,527	0,0905	83
H_4.0Mn	0,0761	0,0429	44
H_4.0Cu	0,028	0,0142	49
H_4.0Ce	0,0205	0,0191	7
H_4.0Fe	0,0093	0,0071	24

Several studies suppose that the mechanism for the decomposition of hydrogen peroxide in the presence of transition metal complexes is the radical mechanism (outer sphere), which was proposed by Haber and Weiss for the Fe(III)–H_2O_2 system [43]. The key features of this mechanism were the discrete formation of hydroxyl and hydroperoxy radicals, which can form a redox cycle with the Fe(II)/Fe(III) couple. In fact, a possible explanation of different transition metal ability of catalyze the H_2O_2 decomposition is related to the adsorption energy of $OH^{\bullet}$ on the metal cation present in the oxide [59].

In our test performed using *t*-BuOH as $OH^{\bullet}$ scavenger (Table 3) it is possible to note that only in the case of Ce-containing glass (H_4.0Ce) the presence of *t*-BuOH do not significantly modify the *k* value (0,0205 vs 0,0191 h^{-1} in the absence an in presence of *t*-BuOH, respectively); in fact, for H_4.0Co the k value deeply decrease from 0.527 h^{-1} (without *t*-BuOH inhibition) to 0.0905 h^{-1} in the presence of *t*-BuOH radical scavenger.

On the basis of *k* value (1st order kinetic) determined in presence/absence of *t*-BuOH as $OH^{\bullet}$ scavenger (Table 3) it is possible to settle that the Ce-containing glass decompose H_2O_2 via a no-radical mechanism (no formation of $OH^{\bullet}$ radical) while the others samples (Co-, Mn-, Cu and Fe-containing glasses) follow mainly a radical pathway via the formation of $OH^{\bullet}$ radical. The $\Delta\%_{inhibition}$ value, reported in Table 3, show the decrease percentage of *k* and this value can be related to the role of $OH^{\bullet}$ radical in the mechanism.

In literature the mechanics proposed for the H_2O_2 decomposition by CeO_2 is not univocally defined, in fact Ce^{4+}/Ce^{3+} redox cycle has also been extended to the oxidation of organic pollutants using ceria as a heterogeneous Fenton-like catalyst. In the presence of H_2O_2, Heckert et al. [60] first confirmed the generation of $OH^{\bullet}$ via Eqs. (1) and (2), analogous to the Fe^{2+}/H_2O_2 Fenton system.

$$Ce^{3+} + H_2O_2 \rightarrow Ce^{4+} + OH^{\bullet} + OH^{-} \tag{1}$$

$$Ce^{4+} + H_2O_2 \rightarrow Ce^{3+} + HO_2^{\bullet} + H^{+} \tag{2}$$
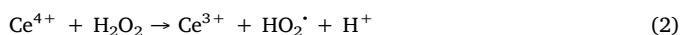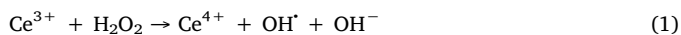
A series of in-depth investigations of the CeO_2/H_2O_2 system by Chen and co-workers [61,62] revealed that the production of $OH^{\bullet}$ radicals critically depends on the oxide surface properties. Without any surface modification, the reaction between Ce^{3+} and H_2O_2 leads to the formation of stable brown peroxide-like species ($Ce^{3+} - OOH^{-}$), which remain stable even at neutral pH and do not directly decompose to generate free $OH^{\bullet}$. The formation of coordinated peroxide species onto CeO_2 nanoparticles was attributed to the oxidation of Ce^{3+} surface ions into Ce^{4+} by H_2O_2 [63], and this process is related to an increment of absorbance in the 400–600 nm range. This is in fully agreement with our results (Fig. 5 section i) where the contact of H_2O_2 solution with H_5.3Ce glass cause the oxidation of Ce^{3+} ions on the glass surface to Ce^{4+} [36]. With this several experimental observation we can conclude that the Ce-containing potential bioactive glasses catalyze the H_2O_2 decomposition *via* a peroxide complex mechanism, which was proposed by Kremer and Stein [44] without the formation of $OH^{\bullet}$, while for the Co, Cu, Mn and Fe-containing glasses the process occurs via $OH^{\bullet}$ radical formation. The significant difference in the peroxide complex mechanism is the two-electron oxidation of two Ce^{3+} ions to two Ce^{4+} ions. The catalytic cycle is completed by the inverse redo process as proposed by Celardo et al. [64].

The catalytic process takes place on the glass surface was confirmed also by the increment of the degradation rate, reducing the glass particles dimensions (Fig. 3 section a) and increasing the specific surface area (Fig. 3 section b).

The different mechanism proposed for Ce-containing glasses can be used to explain the increment of catalytic performance during the 2nd reuse of glass powder in CMA test. In fact, during the first use a portion of Ce^{3+} ions on the glass surface were oxidase to Ce^{4+} in order to reach the optimized Ce^{3+}/Ce^{4+} that enables the catalytic cycle [36,47], in particular as proposed above and by Celardo et al [64] it is necessary to have two cerium ions near with the same oxidation state. During the

2nd reuse the distribution and the oxidation state of cerium ions on the glass surface are optimized and yet at short time, increase the catalytic performance of the glass (see Δ value in Table 3 for H_4.0Ce sample).

However, others factors can contribute to the better catalytic performance during the 2nd immersion in H_2O_2 solution, for example the increase of surface area as a consequence of glass degradation, in fact the glass degradation leads to the formation of pores and cracks on the glass surface; in this way a greater number of transition metals ions (catalytic centres) are in contact with H_2O_2 solution. This effect in visible for all glasses but the effect on the Δ value (Table 3) is small.

Interesting to note that the presence of alginate coating does not modify the catalytic performance of glassy material, this is probably due to the alginate chains functional groups strong interact only with Ca^{2+} ions [65] of the glass surface, these ions do not a significative effect on catalytic H_2O_2 degradation process.

Only H_5.3Co and H_5.3Mn do not show bioactivity in term of HA formation during the SBF soaking until 28 days (Fig. 6). Although Mn-containing bioactive glasses show potential osteoblast growth and osteogenic activity through *in vitro* studies, a negative impact on bioactivity of 45S5 doped with more than 1% mol of MnO_2 was found [66]. Also in the case of cobalt ions (Co^{2+}/Co^{3+}) added to a potential bioactive glass composition the rate of HA formation was reduced [67]. Therefore an adjustment of the concentration of Co and Mn in glass structure must be considered.

The alginate coating delays the HA development but it is not able to inhibit its formation and seem to promote in the case of B_H_5.3Ce and B_K_3.6Ce the catalytic activity toward the H_2O_2 degradation. A possible explanation can be the distorted coordination geometry around the calcium ions that simultaneously must interact both with glass surface and alginate favours the interaction of calcium ions with H_2O_2 molecules and HO_2^{-} ions so promoting its degradation, this factor is maintained also for Ce-containing beads, so the simultaneous presence of cerium and alginate ions increases the efficacy of H_2O_2 degradation, in agreement with the nearly additive behaviour of hydrogen peroxide degradation. We can propose that the beads (glass-alginate composite) are suitable assembly to display bioactivity and enzymatic-like activity.

5. Conclusions

The CMA was verified for all the synthetized samples. The role of the glass composition extremely influences the CMA, in particular the decomposition rate constant *k* decreases in the following order: Co > Mn > Cu > Ce > Fe > V > Ti > Zr with the lowest determined for H glass.

The decomposition follows a 1st order kinetic in the case of H_5.3Co, H_5.3Mn, H_5.3Cu, H_5.3Ce, H_5.3V and H_5.3Fe while a 2nd order kinetic was detected for H, H_5.3Ti and H_5.3V. Between the better catalytic performance, we can proposed a peroxide complex mechanism for the Ce-containing glass while a radical mechanism was proposed for Co-, Cu-, Mn- and Fe-containing glasses with a production of $OH^{\bullet}$ radical. These results can be used when we prototype a possible bioactive glass with antioxidant properties, because if the reduction of a ROS species (such as H_2O_2) was promoted by the formation of another ROS such as $OH^{\bullet}$ radical, this last radical can be negatively interacted with the biological environment causing oxidative stress.

The H_2O_2 soaking (1st immersion) seems to deeply modify the oxidation state of cerium ions in the H_5.3Ce glass, the Ce^{3+} ions on the glass surface are mainly oxidized to Ce^{4+}. This 1st immersion favour the formation of an optimized surface (cerium ions distribution and Ce^{3+}/Ce^{4+} ratio) able to perform a better catalytic performance when we reuse the glass in the CMA tests.

The CMA increase when we reduce the dimension of the sample and increase the specific surface area and the alginate coating (beads) seems do not inhibits the catalytic activity of glass.

The introduction of Ce, Cu, V, Ti, Zr and Fe do not modify the bioactivity in terms of HA formation during SBF tests with respect to the

well know bioactive glass H and the alginate coating delay the HA formation without inhibiting its formation.

H_5.3Co and H_5.3Mn showed the highest value of k but these glasses seem not bioactive until 28 days of SBF soaking, suggesting an adjustment of the concentration of Co and Mn in the glass structure.

In view of the results obtained in the present work, we can conclude that the Ce-containing glasses are the most promising potential bioactive glasses with antioxidant properties in order to decrease the oxidative stress.

Declaration of competing interest

The authors declare that they have no known competing financial interests or personal relationships that could have appeared to influence the work reported in this paper.

Acknowledgements

Appendix A. Supplementary data

Supplementary data to this article can be found online at https://doi.org/10.1016/j.ceramint.2020.07.067.

References

[1] J.M. Anderson, Biological responses to materials, Annu. Rev. Mater. Res. 31 (1) (2001) 81–110, https://doi.org/10.1146/annurev.matsci.31.1.81.

[2] C. Gretzer, L. Emanuelsson, E. Liljensten, P. Thomsen, The inflammatory cell influx and cytokines changes during transition from acute inflammation to fibrous repair around implanted materials, J. Biomater. Sci. Polym. Ed. 17 (6) (2006) 669–687, https://doi.org/10.1163/156856206777346340.

[3] R.K. Murray, Harper's Illustrated Biochemistry, McGraw-Hill Medical ; McGraw-Hill, New York; London, 2009.

[4] L. Sayre, G. Smith, G. Perry, Chemistry and biochemistry of oxidative stress in neurodegenerative disease, Curr. Med. Chem. 8 (7) (2001) 721–738, https://doi.org/10.2174/0929867013372922.

[5] M. Valko, C.J. Rhodes, J. Moncol, M. Izakovic, M. Mazur, Free radicals, metals and antioxidants in oxidative stress-induced cancer, Chem. Biol. Interact. 160 (1) (2006) 1–40, https://doi.org/10.1016/j.cbi.2005.12.009.

[6] E.R. Stadtman, Role of oxidant species in aging, Curr. Med. Chem. 11 (9) (2004) 1105–1112, https://doi.org/10.2174/0929867043365341.

[7] T. Senoner, S. Schindler, S. Stättner, D. Öfner, J. Troppmair, F. Primavesi, Associations of oxidative stress and postoperative outcome in liver surgery with an outlook to future potential therapeutic options, Oxid. Med. Cell. Longev. (2019) 1–18, https://doi.org/10.1155/2019/3950818 2019.

[8] F. Rosenfeldt, M. Wilson, G. Lee, C. Kure, R. Ou, L. Braun, J. de Haan, Oxidative stress in surgery, in: I. Laher (Ed.), Systems Biology of Free Radicals and Antioxidants, Springer Berlin Heidelberg, Berlin, Heidelberg, 2014, pp. 3929–3946, , https://doi.org/10.1007/978-3-642-30018-9_177.

[9] M.-Y. Kang, M. Tsuchiya, L. Packer, M. Manabe, In vitro study on antioxidant potential of various drugs used in the perioperative period, Acta Anaesthesiol. Scand. 42 (1) (1998) 4–12, https://doi.org/10.1111/j.1399-6576.1998.tb05073.x.

[10] J.R. Jones, Review of bioactive glass: from Hench to hybrids, Acta Biomater. 9 (1) (2013) 4457–4486, https://doi.org/10.1016/j.actbio.2012.08.023.

[11] L.L. Hench, The story of Bioglass®, J. Mater. Sci. Mater. Med. 17 (11) (2006) 967–978, https://doi.org/10.1007/s10856-006-0432-z.

[12] L.L. Hench, Opening paper 2015- some comments on Bioglass: four eras of discovery and development, Biomed. Glas 1 (1) (2015), https://doi.org/10.1515/bglass-2015-0001.

[13] L.L. Hench, R.J. Splinter, W.C. Allen, T.K. Greenlee, Bonding mechanisms at the interface of ceramic prosthetic materials, J. Biomed. Mater. Res. 5 (6) (1971) 117–141, https://doi.org/10.1002/jbm.820050611.

[14] C. Rey, C. Combes, C. Drouet, M.J. Glimcher, Bone mineral: update on chemical composition and structure, Osteoporos. Int. 20 (6) (2009) 1013–1021, https://doi.org/10.1007/s00198-009-0860-y.

[15] L.L. Hench, Bioceramics: from concept to clinic, J. Am. Ceram. Soc. 74 (7) (1991) 1487–1510, https://doi.org/10.1111/j.1151-2916.1991.tb07132.x.

[16] V. Mourino, J.P. Cattalini, A.R. Boccaccini, Metallic ions as therapeutic agents in tissue engineering scaffolds: an overview of their biological applications and strategies for new developments, J. R. Soc. Interface 9 (68) (2012) 401–419, https://doi.org/10.1098/rsif.2011.0611.

[17] M. Diba, A.R. Boccaccini, Silver-containing bioactive glasses for tissue engineering

[18] applications, Precious Metals for Biomedical Applications, Elsevier, 2014, pp. 177–211, , https://doi.org/10.1533/9780857099051.2.177.

[18] J.J. Blaker, S.N. Nazhat, A.R. Boccaccini, Development and characterisation of silver-doped bioactive glass-coated sutures for tissue engineering and wound healing applications, Biomaterials 25 (7–8) (2004) 1319–1329, https://doi.org/10.1016/j.biomaterials.2003.08.007.

[19] S.P. Valappil, D. Ready, E.A.A. Neel, D.M. Pickup, W. Chrzanowski, L.A. O'Dell, R.J. Newport, M.E. Smith, M. Wilson, J.C. Knowles, Antimicrobial gallium-doped phosphate-based glasses, Adv. Funct. Mater. 18 (5) (2008) 732–741, https://doi.org/10.1002/adfm.200700931.

[20] S.P. Valappil, D. Ready, E.A. Abou Neel, D.M. Pickup, L.A. O'Dell, W. Chrzanowski, J. Pratten, R.J. Newport, M.E. Smith, M. Wilson, J.C. Knowles, Controlled delivery of antimicrobial gallium ions from phosphate-based glasses, Acta Biomater. 5 (4) (2009) 1198–1210, https://doi.org/10.1016/j.actbio.2008.09.019.

[21] E. Dietrich, H. Oudadesse, A. Lucas-Girot, M. Mami, In vitro bioactivity of melt-derived glass 46S6 doped with magnesium, J. Biomed. Mater. Res. A 88A (4) (2009) 1087–1096, https://doi.org/10.1002/jbm.a.31901.

[22] B.R. Barrioni, A.C. Oliveira, M. de Fátima Leite, M. de Magalhães Pereira, Sol–gel-derived manganese-releasing bioactive glass as a therapeutic approach for bone tissue engineering, J. Mater. Sci. 52 (15) (2017) 8904–8927, https://doi.org/10.1007/s10853-017-0944-6.

[23] B.R. Barrioni, P. Naruphontjirakul, E. Norris, S. Li, N.L. Kelly, J.V. Hanna, M.M. Stevens, J.R. Jones, M.M. de Pereira, Effects of manganese incorporation on the morphology, structure and cytotoxicity of spherical bioactive glass nanoparticles, J. Colloid Interface Sci. 547 (2019) 382–392, https://doi.org/10.1016/j.jcis.2019.04.016.

[24] A. Bari, N. Bloise, S. Fiorilli, G. Novajra, M. Vallet-Regí, G. Bruni, A. Torres-Pardo, J.M. González-Calbet, L. Visai, C. Vitale-Brovarone, Copper-containing mesoporous bioactive glass nanoparticles as multifunctional agent for bone regeneration, Acta Biomater. 55 (2017) 493–504, https://doi.org/10.1016/j.actbio.2017.04.012.

[25] P. Naruphontjirakul, A.E. Porter, J.R. Jones, In vitro osteogenesis by intracellular uptake of strontium containing bioactive glass nanoparticles, Acta Biomater. 66 (2018) 67–80, https://doi.org/10.1016/j.actbio.2017.11.008.

[26] L. Courthéoux, J. Lao, J.-M. Nedelec, E. Jallot, Controlled bioactivity in zinc-doped Sol−Gel-derived binary bioactive glasses, J. Phys. Chem. C 112 (35) (2008) 13663–13667, https://doi.org/10.1021/jp8044498.

[27] V. Aina, G. Malavasi, A. Fiorio Pla, L. Munaron, C. Morterra, Zinc-containing bioactive glasses: surface reactivity and behaviour towards endothelial cells, Acta Biomater. 5 (4) (2009) 1211–1222, https://doi.org/10.1016/j.actbio.2008.10.020.

[28] W. Fan, R. Crawford, Y. Xiao, Enhancing in vivo vascularized bone formation by cobalt chloride-treated bone marrow stromal cells in a tissue engineered periosteum model, Biomaterials 31 (13) (2010) 3580–3589, https://doi.org/10.1016/j.biomaterials.2010.01.083.

[29] D.S. Brauer, N. Karpukhina, M.D. O'Donnell, R.V. Law, R.G. Hill, Fluoride-containing bioactive glasses: effect of glass design and structure on degradation, PH and apatite formation in simulated body fluid, Acta Biomater. 6 (8) (2010) 3275–3282, https://doi.org/10.1016/j.actbio.2010.01.043.

[30] E. Lynch, D.S. Brauer, N. Karpukhina, D.G. Gillam, R.G. Hill, Multi-component bioactive glasses of varying fluoride content for treating dentin hypersensitivity, Dent. Mater. 28 (2) (2012) 168–178, https://doi.org/10.1016/j.dental.2011.11.021.

[31] V. Cannillo, A. Sola, Potassium-based composition for a bioactive glass, Ceram. Int. 35 (8) (2009) 3389–3393, https://doi.org/10.1016/j.ceramint.2009.06.011.

[32] E. Varini, S. Sánchez-Salcedo, G. Malavasi, G. Lusvardi, M. Vallet-Regí, A.J. Salinas, Cerium (III) and (IV) containing mesoporous glasses/alginate beads for bone regeneration: bioactivity, biocompatibility and reactive oxygen species activity, Mater. Sci. Eng. C 105 (2019) 109971, https://doi.org/10.1016/j.msec.2019.109971.

[33] S. Jebahi, H. Oudadesse, H. el Feki, T. Rebai, H. Keskes, P. Pellen, A. el Feki, Antioxidative/oxidative effects of strontium-doped bioactive glass as bone graft. In vivo assays in ovariectomised rats, J. Appl. Biomed. 10 (4) (2012) 195–209, https://doi.org/10.2478/v10136-012-0009-8.

[34] G. Li, S. Feng, D. Zhou, Magnetic bioactive glass ceramic in the system CaO–P_2O_5–SiO_2–MgO–CaF_2–MnO_2–Fe_2O_3 for hyperthermia treatment of bone tumor, J. Mater. Sci. Mater. Med. 22 (10) (2011) 2197–2206, https://doi.org/10.1007/s10856-011-4417-1.

[35] V. Nicolini, E. Gambuzzi, G. Malavasi, L. Menabue, M.C. Menziani, G. Lusvardi, A. Pedone, F. Benedetti, P. Luches, S. D'Addato, S. Valeri, Evidence of catalase mimetic activity in Ce^{3+}/Ce^{4+} doped bioactive glasses, J. Phys. Chem. B 119 (10) (2015) 4009–4019, https://doi.org/10.1021/jp511737b.

[36] V. Nicolini, G. Malavasi, L. Menabue, G. Lusvardi, F. Benedetti, S. Valeri, P. Luches, Cerium-doped bioactive 45S5 glasses: spectroscopic, redox, bioactivity and biocatalytic properties, J. Mater. Sci. 52 (15) (2017) 8845–8857, https://doi.org/10.1007/s10853-017-0867-2.

[37] E.G. Heckert, A.S. Karakoti, S. Seal, W.T. Self, The role of cerium redox state in the SOD mimetic activity of nanoceria, Biomaterials 29 (18) (2008) 2705–2709, https://doi.org/10.1016/j.biomaterials.2008.03.014.

[38] T. Pirmohamed, J.M. Dowding, S. Singh, B. Wasserman, E. Heckert, A.S. Karakoti, J.E.S. King, S. Seal, W.T. Self, Nanoceria exhibit redox state-dependent catalase mimetic activity, Chem. Commun. 46 (16) (2010) 2736, https://doi.org/10.1039/b922024k.

[39] H. Wei, E. Wang, Nanomaterials with enzyme-like characteristics (nanozymes): next-generation artificial enzymes, Chem. Soc. Rev. 42 (14) (2013) 6060, https://doi.org/10.1039/c3cs35486e.

[40] H. Wei, E. Wang, Fe_3O_4 magnetic nanoparticles as peroxidase mimetics and their applications in H_2O_2 and glucose detection, Anal. Chem. 80 (6) (2008) 2250–2254,

https://doi.org/10.1021/ac702203f.

[41] H.J.H. Fenton, LXXIII.—oxidation of tartaric acid in presence of iron, J. Chem. Soc. Trans. 65 (1894) 899–910, https://doi.org/10.1039/CT8946500899 0.

[42] J.H. Baxendale, Decomposition of hydrogen peroxide by catalysts in homogeneous aqueous solution, Advances in Catalysis, vol. 4, Elsevier, 1952, pp. 31–86, , https://doi.org/10.1016/S0360-0564(08)60612-4.

[43] Fritz Haber, J.W. Joseph Weiss, The catalytic decomposition of hydrogen peroxide by iron salts, Proc. R. Soc. Lond. Ser. - Math. Phys. Sci. 147 (861) (1934) 332–351, https://doi.org/10.1098/rspa.1934.0221.

[44] M.L. Kremer, Complex" Versus "Free radical" mechanism for the catalytic decomposition of H2O2 by ferric ions, Int. J. Chem. Kinet. 17 (12) (1985) 1299–1314, https://doi.org/10.1002/kin.550171207.

[45] Z.M. Galbács, L.J. Csányi, Alkali-induced decomposition of hydrogen peroxide, J. Chem. Soc. Dalton Trans. 11 (1983) 2353–2357, https://doi.org/10.1039/DT9830002353.

[46] M. Lombardi, L. Gremillard, J. Chevalier, L. Lefebvre, I. Cacciotti, A. Bianco, L. Montanaro, A comparative study between melt-derived and sol-gel synthesized 45S5 bioactive glasses, Key Eng. Mater. 541 (2013) 15–30 https://doi.org/10.4028/www.scientific.net/KEM.541.15.

[47] V. Nicolini, E. Varini, G. Malavasi, L. Menabue, M.C. Menziani, G. Lusvardi, A. Pedone, F. Benedetti, P. Luches, The effect of composition on structural, thermal, redox and bioactive properties of Ce-containing glasses, Mater. Des. 97 (2016) 73–85, https://doi.org/10.1016/j.matdes.2016.02.056.

[48] S. Leichnitz, J. Heinrich, N. Kulak, A fluorescence assay for the detection of hydrogen peroxide and hydroxyl radicals generated by metallonucleases, Chem. Commun. 54 (95) (2018) 13411–13414, https://doi.org/10.1039/C8CC06996D.

[49] A.J. Werner, Colour Generation and Control in Glass, in: C.R. Bamford (Ed.), Elsevier Scientific Publishing Co., Amsterdam and New York, 1977, p. 224, , https://doi.org/10.1002/col.5080030317 Price, $34.95. Color Res. Appl. 1978, 3 (3), 156–156.

[50] B. Bonelli, M. Armandi, S. Hernandez, S. Vankova, E. Celasco, M. Tomatis, G. Saracco, E. Garrone, The behaviour of an old catalyst revisited in a wet environment: Co ions in APO-5 split water under mild conditions, Phys. Chem. Chem. Phys. 16 (15) (2014) 7074–7082, https://doi.org/10.1039/C4CP00320A.

[51] M. Cerruti, C. Morterra, Carbonate formation on bioactive glasses, Langmuir 20 (15) (2004) 6382–6388, https://doi.org/10.1021/la049723c.

[52] I. Notinghar, J.R. Jones, S. Verrier, I. Bisson, P. Embanga, P. Edwards, J.M. Polak, L.L. Hench, Application of FTIR and Raman spectroscopy to characterisation of bioactive materials and living cells, Spectroscopy 17 (2–3) (2003) 275–288, https://doi.org/10.1155/2003/893584.

[53] C. Satterfield, T. Stein, Decomposition of hydrogen peroxide vapor on relatively inert surfaces, Ind. Eng. Chem. 49 (7) (1957) 1173–1180, https://doi.org/10.1021/ie50571a042.

[54] A. Hiroki, J.A. LaVerne, Decomposition of hydrogen peroxide at Water−Ceramic oxide interfaces, J. Phys. Chem. B 109 (8) (2005) 3364–3370, https://doi.org/10.1021/jp046405d.

[55] J. Goldstein, The kinetics of hydrogen peroxide decomposition catalyzed by cobalt-iron oxides, J. Catal. 32 (3) (1974) 452–465, https://doi.org/10.1016/0021-9517(74)90096-7.

[56] C.M. Miller, R.L. Valentine, Mechanistic studies of surface catalyzed H2O2 decomposition and contaminant degradation in the presence of sand, Water Res. 33 (12) (1999) 2805–2816, https://doi.org/10.1016/S0043-1354(98)00500-4.

[57] W.D. Nicoll, A.F. Smith, Stability of dilute alkaline solutions of hydrogen peroxide, Ind. Eng. Chem. 47 (12) (1955) 2548–2554, https://doi.org/10.1021/ie50552a051.

[58] D.G. Brown, J. Abbot, Effects of metal ions and stabilisers on peroxide decomposition during bleaching, J. Wood Chem. Technol. 15 (1) (1995) 85–111, https://doi.org/10.1080/02773819508009501.

[59] C.M. Lousada, A.J. Johansson, T. Brinck, M. Jonsson, Mechanism of H2O2 decomposition on transition metal oxide surfaces, J. Phys. Chem. C 116 (17) (2012) 9533–9543, https://doi.org/10.1021/jp300255h.

[60] E.G. Heckert, S. Seal, W.T. Self, Fenton-like reaction catalyzed by the rare earth inner transition metal cerium, Environ. Sci. Technol. 42 (13) (2008) 5014–5019, https://doi.org/10.1021/es8001508.

[61] Y. Wang, X. Shen, F. Chen, Improving the catalytic activity of CeO2/H2O2 system by sulfation pretreatment of CeO2, J. Mol. Catal. Chem. 381 (2014) 38–45, https://doi.org/10.1016/j.molcata.2013.10.003.

[62] F. Chen, X. Shen, Y. Wang, J. Zhang, CeO2/H2O2 system catalytic oxidation mechanism study via a kinetics investigation to the degradation of acid orange 7, Appl. Catal. B Environ. 121–122 (2012) 223–229, https://doi.org/10.1016/j.apcatb.2012.04.014.

[63] S.S. Lee, W. Song, M. Cho, H.L. Puppala, P. Nguyen, H. Zhu, L. Segatori, V.L. Colvin, Antioxidant properties of cerium oxide nanocrystals as a function of nanocrystal diameter and surface coating, ACS Nano 7 (11) (2013) 9693–9703, https://doi.org/10.1021/nn4026806.

[64] I. Celardo, J.Z. Pedersen, E. Traversa, L. Ghibelli, Pharmacological potential of cerium oxide nanoparticles, Nanoscale 3 (4) (2011) 1411, https://doi.org/10.1039/c0nr00875c.

[65] K.Y. Lee, D.J. Mooney, Alginate: properties and biomedical applications, Prog. Polym. Sci. 37 (1) (2012) 106–126, https://doi.org/10.1016/j.progpolymsci.2011.06.003.

[66] A.K. Srivastava, R. Pyare, S.P. Singh, In vitro bioactivity and physical–mechanical properties of MnO2 substituted 45S5 bioactive glasses and glass-ceramics, J. Biomater. Tissue Eng. 2 (3) (2012) 249–258, https://doi.org/10.1166/jbt.2012.1043.

[67] B.R. Barrioni, E. Norris, J.R. Jones, M.M. de Pereira, The influence of cobalt incorporation and cobalt precursor selection on the structure and bioactivity of sol–gel-derived bioactive glass, J. Sol. Gel Sci. Technol. 88 (2) (2018) 309–321, https://doi.org/10.1007/s10971-018-4823-7.